CHINESE OPTICS LETTERS

Vol. 21, No. 8 | August 2023

Spatiotemporal optical vortices generation in the green and ultraviolet via frequency upconversion [Invited]

Xuechen Gao (高雪晨)[1,†], Yuwei Zhao (赵雨薇)[2,†], Jue Wang (王 珏)[1], Yang Lu (卢 扬)[1], Jiaxuan Zhang (张家璇)[1], Jintao Fan (范锦涛)[1*], and Minglie Hu (胡明列)[1**]

[1] Ultrafast Laser Laboratory, Key Laboratory of Opto-electronic Information Science and Technology of Ministry of Education, School of Precision Instruments and Opto-electronics Engineering, Tianjin University, Tianjin 300072, China

[2] Science and Technology on Electro-Optical Information Security Control Laboratory, Tianjin 300308, China

*Corresponding author: fanjintao@tju.edu.cn

**Corresponding author: huminglie@tju.edu.cn

Received April 29, 2023 | Accepted June 15, 2023 | Posted Online August 7, 2023

As a newly discovered type of structured light, a spatiotemporal optical vortex (STOV), which is remarkable for its space–time spiral phase and transverse orbital angular momentum (OAM), has garnered substantial interest. Most previous studies have focused on the generation, characterization, and propagation of STOVs, but their nonlinear frequency conversion remains largely unexplored. Here, we experimentally demonstrate the generation of green and ultraviolet (UV) STOVs by frequency upconversion of a STOV carried near-infrared (NIR) pulse emitted by a high repetition rate Yb-doped fiber laser amplifier system. First, we verify that the topological charge of spatiotemporal OAM (ST-OAM) is doubled along with the optical frequency in the second-harmonic generation (SHG) process, which is visualized by the diffraction patterns of the STOVs in the fundamental and second-harmonic field. Second, the space–time characteristic of NIR STOV is successfully mapped to UV STOV by sum-frequency mixing STOV at 1037 nm and Gaussian beams in the green band. Furthermore, we observe the topological charges of the ST-OAM could be degraded owing to strong space–time coupling and complex spatiotemporal astigmatism of such beams. Our results not only deepen our understanding of nonlinear manipulation of ST-OAM spectra and the generation of STOVs at a new shorter wavelength, but also may promote new applications in both classical and quantum optics.

Keywords: ultraviolet spatiotemporal optical vortex; second-harmonic generation; sum-frequency generation.
DOI: 10.3788/COL202321.080004

1. Introduction

Since its first experimental demonstration, spatiotemporal optical vortices (STOVs), characterized by phase singularity in the space–time domain, have emerged as a prominent topic in optics[1,2]. The novel wave packets with controllable transverse orbital angular momentum (OAM) have attracted considerable interest owing to their analogies with many physical systems, including tropical cyclones, plasmonic physics, magnetic nanowires, and more[3–5]. Very recently, the diffraction properties of STOV were demonstrated both theoretically and experimentally. A diffraction rule that the topological charge can be witnessed according to a gap number of STOV diffraction modes was uncovered[6]. Such a fast recognition technique of STOVs may enable important and wide applications. Almost at the same time, Chen *et al.* achieved degradation-free STOV with transverse OAM (TOAM) beyond 10^2 by using immediate x–ω modulation. In addition, time diffraction-free spatiotemporal OAM was also observed with the help of dispersion engineering[7,8]. Apart from their fundamental importance, this new type structured beam may lead to revolutions in the field of applications, for example, optical communication and quantum optics[9,10]. Nevertheless, to explore the extra space–time degree of freedom provided by STOVs for new intriguing applications, it is particularly appealing for accessing such wave packets in different spectral regions.

Second-order optical nonlinear processes where the light strongly interacts with material to generate light at new frequencies are one of the most attractive research directions for many classical and quantum applications. According to the intrinsic spatiotemporal coupling mechanism, mode degradation exists during propagation, and hence the nonlinear manipulation of the TOAM becomes more complicated compared with the conventional OAM, where the OAM is parallel to propagation direction of light. Recently, the second-harmonic generation (SHG) of STOVs has been experimentally realized[11,12].

When the optical frequency of STOV is doubled ($\omega - 2\omega$), the topological charge doubles simultaneously ($l - 2l$). It means that second-harmonic pulses will carry twice the TOAM of the fundamental pulses. The conversion rule observed is analogous to the conventional OAM.

Despite these successes, the existing methods have faced the biggest challenge, that is, inefficiencies in the second-harmonic light extraction process due to the lack of a focusing system. This is of particular importance when the repetition rate of the injection laser is several tens of megahertz. On the other hand, the generation and characterization in the ultraviolet (UV) spectral domain have not been addressed yet. The realization of STOVs in the UV region may inspire applications such as microscopy, laser writing, and holography. To access the UV spectral region, sum frequency generation (SFG) shifting infrared (IR) and visible (VIS) to UV is more promising owing to the strict requirement on the machining accuracy of the phase mask at the shorter wavelength. However, it remains a big challenge to achieve SFG of STOVs because SFG is driven by two ultrafast laser pulses with different TOAM and time delay with respect to each other. Therefore, it is significant to further investigate the nonlinear frequency conversion processes of STOVs.

In this Letter, we demonstrate experimentally the generation of green- and UV-STOVs during two frequency upconversion processes. The first one is SHG of the fundamental STOVs in the near-IR (NIR). The second one is upconversion of STOVs from NIR to UV via SFG mixing IR-STOV and green Gaussian beams. We find that the space–time topological charge obeys the same charge conservation and nonlinear scaling rules as observed before. That is to say, the topological charge doubling is realized in the SHG, and the properties of the driving IR-STOVs are directly mapped into UV when the VIS is Gaussian in the SFG. Due to the unavailability of a suitable reference beam[13] at shorter wavelengths, especially in the UV, we were not able to record the time-varying interference pattern to recognize the topological charge of the generated STOVs. Therefore, the diffraction patterns of STOV pulses are measured to identify the topological charges of STOVs in different spectral regions. Moreover, we also show that the topological structures in both types of frequency upconversion processes may not be conserved. Mode degradation could be observed only by tuning the position of the nonlinear crystal along the optical path due to the temporal diffraction and strong space–time coupling nature of the STOVs. Our findings suggest the possibilities of nonlinear manipulation of ST-OAM spectra and the generation of STOVs in the shorter wavelength range, which have potential applications in the fields of STOV-based optical communications and quantum optics.

2. Generation of Second-harmonic STOVs

The experiment for the generation and characterization of second-harmonic STOVs is sketched in Fig. 1. The fundamental laser pulses (1037 nm, 200 fs) with an average output power up to 4.2 W are delivered from a home-built Yb^{3+} doped

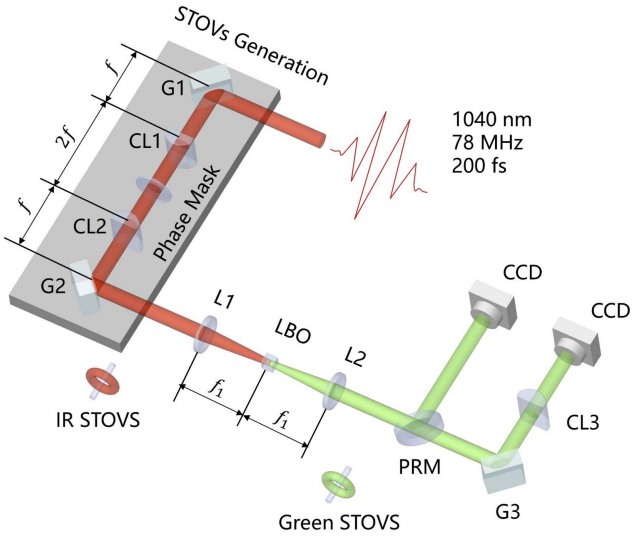

Fig. 1. Experimental setup for the generation and characterization of second-harmonic STOVs. Fundamental STOVs of topological charges l = 1, 2 in the NIR are generated by a custom 4-f pulse shaper. G, grating; CL, cylindrical lens; L, lens; LBO, lithium triborate crystal; PRM, partial reflection mirror; CCD, charge-coupled device.

femtosecond fiber amplifier system operating at 78 MHz. The fundamental pulse is directed to a custom 4-f pulse shaper composed of two diffraction gratings (1200 lines/mm), two cylindrical lenses ($f = 100$ mm), and one phase mask, where the STOV in the NIR is created. Similar to that described in Refs. [1,2], the phase plate located in the two-dimensional Fourier (x–ω) plane of the pulse shaper is employed to load spiral phase to the incident wave packet. By changing different phase masks, the STOVs with topological charges $l = +1, +2$ could be obtained, respectively. Then, a second-harmonic STOV is achieved by focusing the fundamental laser with a beam diameter of ~2 mm to a 2.5 mm thick type-I LiB_3O_5 (LBO) crystal via a focal lens, L1, with a focal length of $f_1 = 100$ mm. The generated green STOV is collimated using another lens (L2, $f = 100$ mm). The green STOV intensities are measured after passing through dichroic mirrors, and the topological charges are characterized based on its diffraction properties. Because of the fast detection method, there is no need to stretch the fundamental wave (FW) to the picosecond time scale, leading to higher nonlinear conversion efficiencies. The setup is similar to that in Ref. [6], the emitted second harmonics are collected by a lens, a grating (1200 lines/mm, blaze wavelength 520 nm), another cylindrical lens, and a commercially available CCD. The generated green STOV has an average output power of about 80 mW.

To detect the fundamental STOVs, a flip gold-coated mirror is used to reflect it from the main optical path. The intensity profile of the STOVs at 1037 nm is measured by CCD first. As shown in the first column of Figs. 2(a) and 2(b), the intensity profiles and corresponding diffraction patterns of STOVs with topological charges $l = 1$ and $l = 2$ are displayed, respectively. The intensity profiles appear as a gap between two circles, which is attributed to the spatiotemporal phase singularity. Given the time-to-space

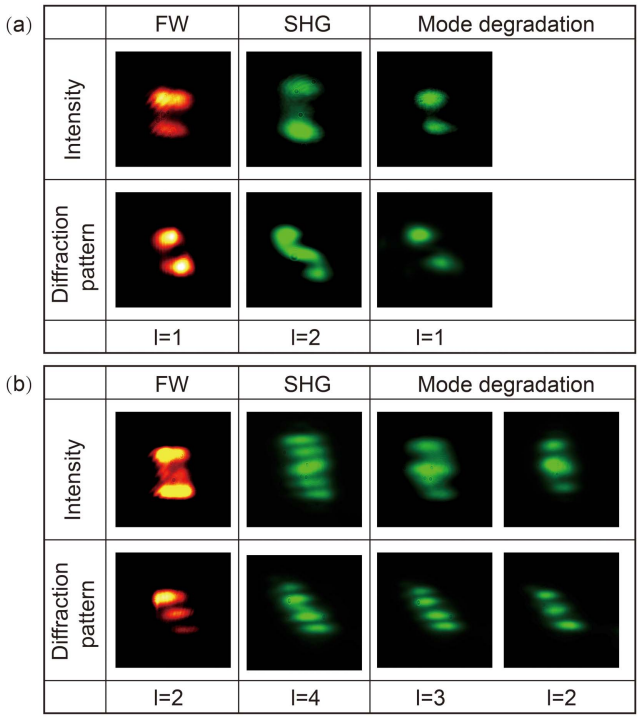

Fig. 2. (a) and (b) show experimental results of the green STOVs generated by the FW with topological charges of l = 1 and l = 2, respectively.

mapping process, the time-varying phase in the space–time domain can be converted to the intensity distribution in the space domain. To this end, the topological charges are verified directly and rapidly by the diffraction patterns in the witness plane using the diffraction method[3]. In analogy with traditional OAM, the number of dark lines indicates the absolute value of the topological charge[14].

In the second column of Figs. 2(a) and 2(b), we show the intensity distribution and diffraction patterns of the second-harmonic STOVs with the order of $l = 2$ and 4, respectively. Compared with the previous works[11,12], we put the nonlinear crystal in the focal plane, which means a spatial Fourier transform is performed. According to the theory in Ref. [15], such an additional spatial Fourier transform is required to covert the spiral phase onto the x–t plane. Therefore, we can see that around a certain position, the topological change doubling along with the optical frequency doubling of second-harmonic STOVs is observed. The nonlinear scaling rule found here is similar to that in Refs. [10,11], where the topological charges are doubling in the SHG process. When the topological charge of fundamental STOVs is $l = 1$ ($l = 2$), the topological charge of the green STOVs is $l = 2$ ($l = 4$), which can be indicated from the gap numbers in the diffraction patterns of the green STOVs. As can be seen from Fig. 2, the intensity profiles of the green STOVs are different from those of the fundamental STOVs. More separated lobes appear even in the intensity profiles. We attribute this to high time diffraction and large interaction length of the LBO crystal, leading to strong spatiotemporal astigmatism in dispersive material. As a result, a higher degree of distortion occurs when the topological order of the STOVs increases.

More interesting cases are mode degradation in the SH process by changing the position of the LBO, as displayed in the last column of Figs. 2(a) and 2(b). The nonlinear scaling rule cannot be fulfilled. We note that spatial Fourier transform is performed here. Given that the transform is completely only in a certain position (focal plane), the STOVs will degrade at other positions. Therefore, we tune the position of the crystal away from the focal plane. When the STOV with topological charge $l = 1$ is severed as an FW, green STOVs with topological charge $l = 2$ and $l = 1$ can be obtained. When increasing the topological charge of the FW to 2, more complicated situations can be stimulated. Counting the number of gaps in diffraction patterns in Fig. 2, the generated green STOV possesses topological charges ranging from 2 to 4. The mode degradation observed here is mainly caused by strong space–time coupling of the STOVs and temporal walk-off between the NIR and green beams in the dispersive medium. Note that the temporal walk-off influences the overlap part of the interaction beams in the time domain, and the STOVs naturally show time-varying phases along propagation. Going forward, as described in Ref. [16], the TOAM is shared between a photon and a STOV polariton, resulting in integer multiples of topological charges of a parameter that depends on the STOV symmetry and the group velocity dispersion. This mode decomposition will lead to mode degradation when parts of the topological charge participates in the SHG or SFG process. Our findings suggest that additional phase singularities could be realized in the SHG process, which offer an alternative to nonlinear manipulation of the ST-OAM spectra of light.

3. Generation of UV-STOVs by SFG Process

The experimental setup for the generation of UV-STOVs is shown in Fig. 3. The laser source is exactly the same as the one used in the SHG process. The pulses are first sent through

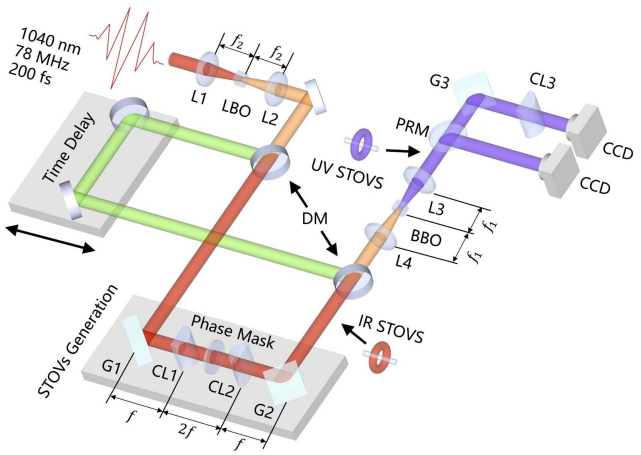

Fig. 3. Experimental setup for the generation and characterization of UV STOVs. DM, dichroic mirror.

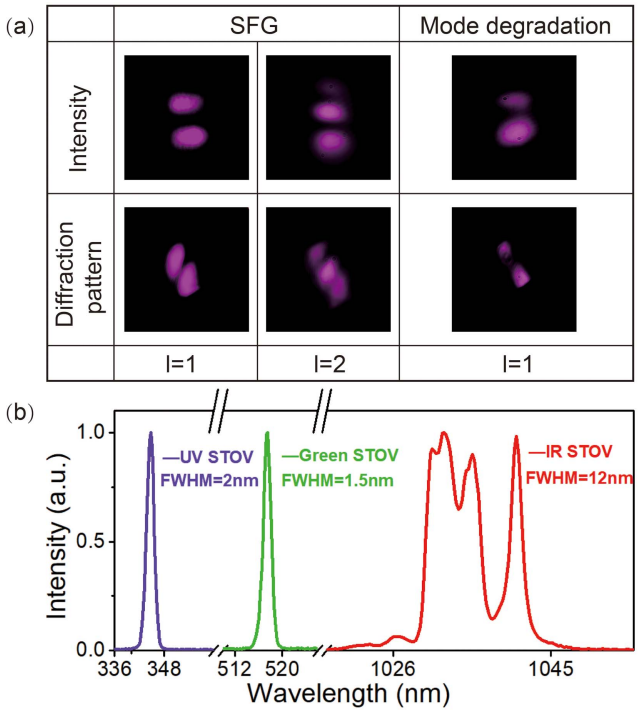

Fig. 4. (a) Measured intensity profile and the corresponding diffraction lobe pattern of the UV-STOVs with topological charges l = 1, 2; (b) spectra of UV STOV, green Gaussian, and IR STOV.

a 2.5 mm thick type-I LBO crystal, emitting the undepleted fundamental and second harmonic. Then, these two beams are spatially separated in a bichromatic Mach–Zehnder interferometer, which is utilized to manipulate two beams individually before focusing into a 2 mm beta-barium borate (BBO) crystal. The beam diameters of the NIR STOVs and the green Gaussian are set to be ~2.5 mm. L3 ($f = 100$ mm) and L4 ($f = 100$ mm) are two focusing and collimating lenses used for SFG, respectively. One arm is used to load STOV in the NIR pulses. More detailed description can be found above. No ST-OAM operates on the second-harmonic beam. These two beams are then spatially and temporally combined to drive SFG in the BBO. The angle between the two beams can also be well adjusted by translating the last mirror of each arm. The UV-STOV intensities are measured, and the topological charges are characterized. The emitted third harmonics are collected by a lens, a grating (1200 lines/mm, blaze wavelength 350 nm), another cylindrical lens, and a UV CCD camera.

UV STOVs at 346 nm are generated by simultaneously sending the IR STOVs and VIS Gaussian beams into the BBO crystal. The spectra of driving IR-STOV, green Gaussian, and UV-STOV are displayed in Fig. 4(b). The spectral bandwidth for the NIR and UV beams is 12 and 2 nm, respectively. In this part, we first study the SFG process in the optimum focusing condition. To compensate for the walk-off between two driving pulses, noncollinear phase matching is preferred by slightly changing the incident angle of the VIS components. Both the intensity profiles and diffraction patterns are shown in Fig. 4(a). We discern that the dispersion and time diffraction could result in spatiotemporal astigmatism in ST-OAM pulses. However, by adjusting the incident angle well, as well as by time delay, the resulting UV STOVs still share the same topological charge as the IR STOVs, which are in good agreement, as predicted by theory in Ref. [6]. As is obvious in Fig. 4(a), when the FW topological charge is $l = 1$ ($l = 2$), the topological charge of the generated UV should be $l = 1$ ($l = 2$). To achieve high-quality UV STOVs, the combined beams are weakly focused into the BBO crystal, resulting in lower power density, and thus SFG efficiency is relatively low. On the other hand, the beam modes of the fundamental beam and green beam are different; as a result, two beams could not overlap well. For the green Gaussian beam, the maximum intensity is located at the center, while for the STOVs, the intensity exhibits time-varying property, and different parts of the beam have different overlapped parts. Therefore, the nonlinear conversion efficiency is rather low: the maximum average output power is around 50 mW with 3.7 W input power. In the future, high-power UV STOVs could be achieved by increasing the pump power intensity through using a high-power pump laser source and tighter focusing. Moreover, since two beams have different propagation properties, we can use two different focus lenses to make better overlap conditions for the two beams. We therefore confirm the nonlinear scaling rule. Given that the ST-OAM is conserved in the SFG process, we can produce UV-STOVs with higher topological charges by increasing the topological orders of both the fundamental beam and the SHG beam.

We also study the mode degradation phenomenon in the SFG process when the topological charge of the IR-STOVs is $l = 2$. In this case, the effect of time diffraction will lead to the decomposition of an $l = 2$ STOV when only part of the IR-STOV is in superposition with the green Gaussian beam. The diffraction pattern with only one gap indicates that the UV-STOV has a confirmed spatiotemporal topological charge of $l = 1$, as shown in Fig. 4(a).

4. Conclusion

In conclusion, we have successfully demonstrated the STOV generation in the shorter wavelength regions (green and UV) by nonlinear upconversion of an NIR STOV. By defining the topological charge of the STOVs using the diffraction method, we find the conservation of space–time topological charge of STOVs. By comparing the SHG and SFG processes, we can conclude that ST-OAM carried light obeys the same nonlinear scaling rules as the conventional OAM of light. Mode degradations are also observed in both processes, which offer an alternative to nonlinear manipulation of the ST-OAM spectra at new shorter wavelengths. Should a quasi-phase-matched crystal with a finely designed period-poled structure be used, it is possible to realize a nonlinear upconversion process with improved efficiency. We anticipate that our work opens up new opportunities for high-dimensional laser processing and quantum optics.

Acknowledgement

This work was supported by the National Natural Science Foundation of China (NSFC) (Nos. 62105237, 61827821, and 62227821).

†These authors contributed equally to this work.

References

1. S. W. Hancock, S. Zahedpour, A. Goffin, and H. M. Milchberg, "Free-space propagation of spatiotemporal optical vortices," Optica **6**, 1547 (2019).
2. A. Chong, C. Wan, J. Chen, and Q. Zhan, "Generation of spatiotemporal optical vortices with controllable transverse orbital angular momentum," Nat. Photonics **14**, 350 (2020).
3. P. Peduzzi, B. Chatenoux, H. Dao, A. De Bono, C. Herold, J. Kossin, F. Mouton, and O. Nordbeck, "Global trends in tropical cyclone risk," Nat. Clim. Change **2**, 289 (2012).
4. S. S. P. Parkin, M. Hayashi, and L. Thomas, "Magnetic domain-wall racetrack memory," Science **320**, 190 (2008).
5. Y. Fang, S. Lu, and Y. Liu, "Controlling photon transverse orbital angular momentum in high harmonic generation," Phys. Rev. Lett. **127**, 273901 (2021).
6. S. Huang, P. Wang, X. Shen, J. Liu, and R. Li, "Diffraction properties of light with transverse orbital angular momentum," Optica **9**, 469 (2022).
7. K. Y. Bliokh and F. Nori, "Spatiotemporal vortex beams and angular momentum," Phys. Rev. A **86**, 033824 (2012).
8. K. Y. Bliokh, "Spatiotemporal vortex pulses: angular momenta and spin-orbit interaction," Phys. Rev. Lett. **126**, 243601 (2021).
9. A. Forbes, S. Ramachandran, and Q. Zhan, "Photonic angular momentum: progress and perspectives," Nanophotonics **11**, 625 (2022).
10. J. Chen, C. Wan, and Q. Zhan, "Engineering photonic angular momentum with structured light: a review," Adv. Photonics **3**, 064001 (2021).
11. G. Gui, N. J. Brooks, H. C. Kapteyn, M. M. Murnane, and C. Liao, "Second-harmonic generation of spatiotemporal optical vortices and conservation of orbital angular momentum," Nat. Photonics **15**, 608 (2021).
12. S. W. Hancock, S. Zahedpour, and H. M. Milchberg, "Second-harmonic generation of spatiotemporal optical vortices and conservation of orbital angular momentum," Optica **8**, 594 (2021).
13. S. W. Hancock, S. Zahedpour, and H. M. Milchberg, "Transient-grating single-shot supercontinuum spectral interferometry (TG-SSSI)," Opt. Lett. **46**, 1013 (2021).
14. P. Vaity, J. Banerji, and R. P. Singh, "Measuring the topological charge of an optical vortex by using a tilted convex lens," Phys. Lett. A **377**, 1154 (2013.)
15. W. Chen, W. Zhang, Y. Liu, F. Meng, J. M. Dudley, and Y. Lu, "Time diffraction-free transverse orbital angular momentum beams," Nat. Commun. **13**, 4021 (2022).
16. S. W. Hancock, S. Zahedpour, and H. M. Milchberg, "Mode structure and orbital angular momentum of spatiotemporal optical vortex pulses," Phys. Rev. Lett. **127**, 193901 (2021).